Available online at www.sciencedirect.com
ScienceDirect
Journal of Solid State Chemistry 179 (2006) 3942–3948
JOURNAL OF SOLID STATE CHEMISTRY
www.elsevier.com/locate/jssc

Structure of sputtered Co–Se thin films prepared for an application in catalysis

L. Zhu[a], D. Susac[a], A. Lam[a], M. Teo[a], P.C. Wong[a], D. Bizzotto[a], S.A. Campbell[b], R.R. Parsons[c], K.A.R. Mitchell[a,*]

[a]*Department of Chemistry, University of British Columbia, 2036 Main Mall, Vancouver, BC, Canada V6T 1Z1*
[b]*Ballard Power Systems Inc., 9000 Glenlyon Parkway, Burnaby, BC, Canada V5J 5J9*
[c]*Department of Physics and Astronomy, University of British Columbia, 6224 Agricultural Road, Vancouver, BC, Canada V6T 1Z1*

Received 22 June 2006; received in revised form 23 August 2006; accepted 26 August 2006
Available online 1 September 2006

Abstract

Co–Se thin films prepared by magnetron sputtering have shown significant activity for the oxygen reduction reaction. One sample, after sectioning by ultramicrotomy, was studied by high-resolution scanning transmission electron microscopy (HRSTEM) and scanning Auger microscopy (SAM), and X-ray diffraction (XRD) was used for characterizing further samples. These thin films were shown to have Co–Se nanocrystals embedded into Se-rich matrices. The TEM and XRD results were consistent with the nanocrystallites being non-stoichiometric with structures related to those of monoclinic $Co_{1-x}Se$ ($x = 0.125$–0.25).

Keywords: Co–Se thin films; Magnetron sputtering; Fuel cell catalyst; Transmission electron microscopy; X-ray diffraction; Scanning auger microscopy

1. Introduction

The proton exchange membrane fuel cell (PEMFC) is a promising candidate for future non-polluting vehicle propulsion [1–3], but among current challenges are the cost of the Pt-based catalysts used [4,5] and their slow kinetics for the oxygen reduction reaction (ORR) [6]. Such factors have encouraged searches for developing cheaper non-precious metal catalysts that can display sufficient activity for ORR in acidic media. Pioneering work by Alonso-Vante and Tributsch [7–9] on catalysts containing Ru, Mo, and Se (including chevrel phase compounds) showed promise for ORR, although the use of Ru does not obviate the cost issue for mass production. Very recently, model thin-film materials formed from Co and Se have also been shown to have significant activity for ORR, with Tafel slopes comparable to that of Pt, although the current densities are at least two orders of magnitude less than for a Pt thin-film electrode [10].

To help guide the search for new non-precious metal catalysts, it is important to know how the chalcogen-based catalysts work, and for that an important ingredient is their structure. This paper addresses that particular point for a thin-film sample of average composition Co(44%)Se(56%) which has been studied as an electrocatalyst for ORR [10]. The prime structural techniques applied to this thin-film structure are high-resolution scanning transmission electron microscopy (HRSTEM) and X-ray diffraction (XRD), but important analytical characterizations are also made with scanning Auger microscopy (SAM) and energy-dispersive X-ray (EDX) spectroscopy. A comparison with XRD is also included for a separate sample of overall composition Co(28%)Se(72%). All these thin-film compositions (atomic %) apply to the as-prepared samples, but the results reported apply to samples that have previously undergone electrochemical dynamic polarization measurements, where each thin film was used as a rotating disc electrode [10].

2. Experimental

The Co–Se thin films used in this study were formed by magnetron sputtering onto a disk-shaped glassy-carbon

*Corresponding author. Fax: +1 604 822 2847.
E-mail address: karm@chem.ubc.ca (K.A.R. Mitchell).

0022-4596/$ - see front matter © 2006 Elsevier Inc. All rights reserved.
doi:10.1016/j.jssc.2006.08.028

substrate. Before the deposition, each substrate (working area 1.23 cm^2) was polished with SiC paper (P4000 Microcut, Buehler) and that was followed by polishing with 6 and 1 μm diamond suspensions (Leco) sprayed on the polishing microcloths (Buehler). Ultrasonic rinsing in deionized water was applied between each polishing stage and in acetone (HPLC grade, Fisher Scientific) for 2 min after the final step. The thin films were prepared in a sputter coater system (model V3 T, Corona Vacuum Coaters Inc.) using either dual deposition from elemental targets (Co 99.95% purity, Kurt Lesker; gray Se 99.99% purity, Angstrom Sciences) or single deposition from a Co–Se composite target. The latter was fabricated by mixing equal weights of Co powder (~100 mesh, 99.9% purity, Aldrich) and Se pellets (~2 mm dimension, 99.999% purity, Aldrich) and then melting in a mold (diameter 5 cm). The Co target was sputtered in the direct current (dc) mode, while the radio frequency (rf) mode was applied for the Se and Co–Se composite targets. The composition of the deposited film was controlled by varying the powers applied to the targets, and the deposition time was adjusted to obtain films with ~0.5 μm in thickness. Before film deposition, the system was pumped to 3×10^{-6} Torr, but the plasma discharge was operated at 3.5×10^{-3} Torr with a continuous throttled Ar flow (25 $cm^3 min^{-1}$). The sputtering targets were pre-sputtered for 10 min before moving the sample into the deposition zone. A bias of −180 V was applied to the substrate for the first minute of film preparation, while −75 V was used for the rest of the deposition.

The overall compositions of the deposited films were determined by EDX spectroscopy using a Hitachi S2300 spectrometer (20 keV incident electron beam); measured elemental peak areas in the EDX spectra were converted into percentage atomic compositions using the Quartz XONE software. Surface characterizations were made by measuring Auger electron spectra by SAM with a Microlab 350 instrument (Thermo Electron Corp.) fitted with a field emission electron source and hemispherical energy analyzer. The latter instrument also allowed measurements with scanning electron microscopy (SEM). The Auger spectra were measured, in both area and point analysis mode, with the primary electron beam at 10 keV and 3.5 nA.

Thin cross-sections were required for the study with HRSTEM. The initial cuts were made manually from a Co–Se thin film using an ultra-clean diamond knife, and each strip was mounted in a polyethylene capsule parallel to the capsule's axis. The encapsulating epoxy resin was formed from Epon 812, Araldite 6005, DDSA (dodenyl succinic andydride) and DMP-30 in volumes 30, 10, 12.5, and 1.25 mL, respectively; curing was done at 57 °C for 72 h. An ultramicrotome (MT6000 Sorvall) with diamond knife was used to make the cross-sections (cutting angle ~45°, clearance angle 2°). The cutting speed and section thickness were set at 0.1 mm s^{-1} and 25 nm, respectively. The slices produced were collected from a bath of double-distilled water onto 400 mesh TEM copper grids and later dried at room temperature. The cross-sectioned samples were analyzed by HRSTEM (the simpler acronym TEM is used in the following) with a Tecnai G^2 instrument (FEI) at Simon Fraser University. This instrument is equipped with a field emission source (F20 model) operating at 200 kV for imaging, diffraction, and EDX. Before measurements, this instrument was calibrated with a Au standard sample provided by the manufacturer.

Step-scan X-ray powder diffraction data were collected (2θ range 2–90°) using Cu$K\alpha$ radiation on a Bruker D8 Bragg-Brentano diffractometer equipped with a diffracted-beam graphite monochromator crystal. The samples were mounted such that the thin-film (electrode) surfaces were level with the diffracting plane of the standard sample holder, and they were rotated during data collection to improve the statistics. The measurements were made in steps of 0.02° with total measurement times ranging from 1.2 to 6.4 h. To check the measurement precision, the XRD pattern from a particular Co–Se thin film was measured simultaneously with a measurement for quartz. This was accomplished by filling the region neighboring the Co–Se film with a quartz-Vaseline paste that was leveled to the main sample so that during rotation (after mounting on a standard Bruker sample holder) both the paste and the Co–Se sample interacted with the X-ray beam. Before measurements, the XRD instrument was calibrated with a NIST 1976 XRD flat-plate intensity corundum standard (Bruker).

3. Results and discussion

3.1. Ultramicrotomed thin film studied by TEM

A large-area SEM image of the ultramicrotomed sample, of overall composition Co(44%)Se(56%), is shown in Fig. 1 after depositing onto a Cu grid used as the substrate for TEM. The thin-film cross-section is identified as the region sandwiched between the fibrous glassy-carbon area and the epoxy resin; the box in white outline shows the part of the film studied by TEM and SAM. Fig. 2 compares the Auger electron spectra measured from this local area on the film with measurements made from the original thin film after the electrochemical testing for ORR catalytic activity. The Co LMM transitions occur with kinetic energies in the 620–800 eV range with the most intense peak at 773.0 eV, while the Se LMM transitions occur from 1160 to 1360 eV with the most intense peak at 1309.8 eV. The Auger peak locations and shapes measured from the ultramicrotome sample are consistent with those taken from the thin film before sectioning, and that helps support the view that the preparation process for TEM analysis has not altered the chemical state of the Co–Se thin film.

Fig. 3a shows a high magnification SEM image from the cross-section of the sample of overall composition Co(44%)Se(56%), which had been identified in Fig. 1. The film exhibits columnar structure which is commonly observed when the deposited atoms have limited mobility [11]. The TEM image in Fig. 3(b) demonstrates that the

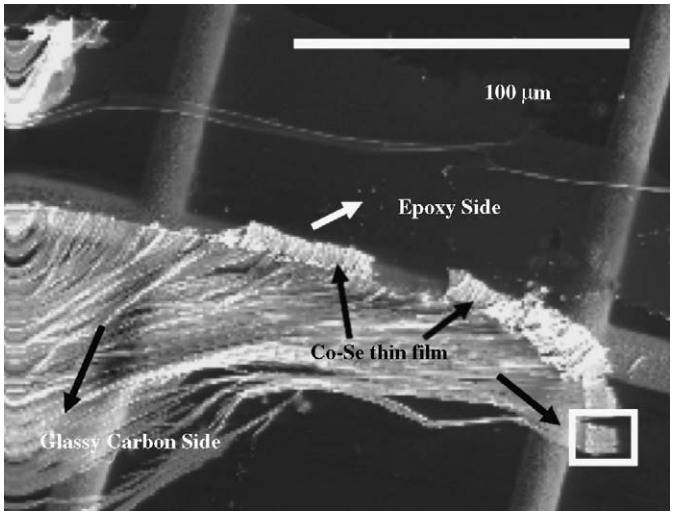

Fig. 1. Scanning electron micrograph of ultramicrotomed thin-film sample of composition Co(44%)Se(56%) prepared for TEM analysis.

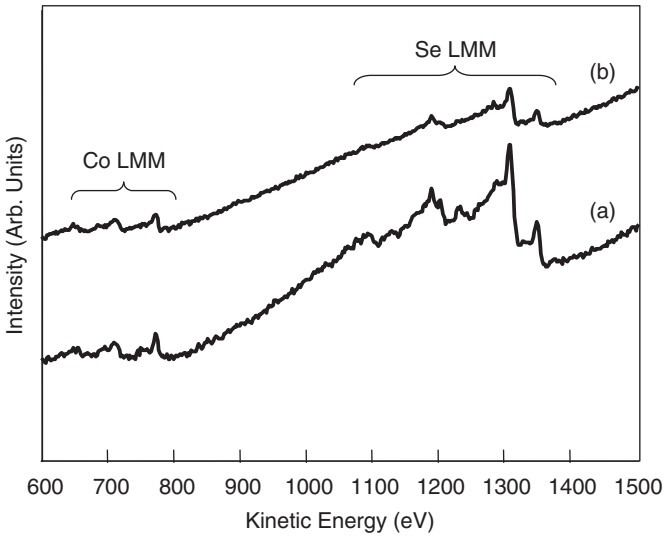

Fig. 2. Auger electron spectra from thin-film sample of composition Co(44%)Se(56%): (a) before sectioning, and (b) after sectioning for TEM analysis.

columns are up to 500 nm long and 200 nm wide. Fig. 3(c) shows a selected area (marked by the white circle in Fig. 3(b)) at the outermost part of the film that had previously been exposed to acid during the electrochemical examination of catalytic activity. The presence of numerous small black nanoparticles (~20 nm diameter) separated by lighter regions is seen, and the TEM image with highest resolution from this area (Fig. 3(d)) shows clear grain orientations. The lighter domains can be divided into ordered (sites 1) and disordered (sites 2) regions, while the dark domains (sites 3) are always ordered. EDX showed that the lighter regions are very rich in Se whereas the small dark regions contain both Co and Se (Fig. 4). Diffraction patterns from these areas (around 20 nm × 20 nm) show that the small dark regions are polycrystalline (Fig. 5(a)), while the lighter regions are amorphous (Fig. 5(b)). This information together supports the view that the sputtered thin film has Co–Se nanocrystals embedded into a Se-rich matrix, with the latter being basically amorphous while having some partial ordering (as for region 1 in Fig. 3(d)). This is consistent with the SAM analysis in previous work [10] which indicated that surfaces of Co–Se thin films become very rich in Se after electrochemical processing. It is known that Se itself does not have significant activity for ORR [12–14], and that leads to the conclusion that the catalytic activity from the sputtered Co–Se thin film must be primarily associated with the nanoparticles, which appear as "black dots" in Fig. 3(c).

In order to probe further the structure of the nanocrystals, the *d*-spacings of several individual particles (dimension 5–20 nm) were measured, and the ranges of their values are listed in Table 1, where they are compared against two reference compounds. This comparison suggests that the nanoparticles detected by TEM from the sample with overall composition Co(44%)Se(56%) match to a good degree with the structure of monoclinic Co_7Se_8, and this is followed up further with XRD.

3.2. XRD characterizations

Several Co–Se thin films (all of thickness $\leqslant 0.50\,\mu m$) were prepared by magnetron sputtering, and Fig. 6 reports XRD diffractograms from two of them after electrochemical characterization, as well as another from a glassy-carbon substrate on which no film had been deposited. The particular thin films shown in Fig. 6 include that of overall composition Co(44%)Se(56%) studied by TEM and another of composition Co(28%)Se(72%). Since the XRD patterns of all the thin films studied are similar, these two films are taken as representative of all samples, whose as-prepared bulk compositions (determined by EDX) ranged from Co(28%)Se(72%) to Co(73%)Se(27%). The diffractograms from all films include contributions from the glassy carbon, namely broad peaks near 26° and 43°, while signals close to 33.5° and 44.6° result from the Co–Se thin films (although for the example in Fig. 6 for composition Co(28%)Se(72%) the peak near 44.6° appears as a shoulder on the nearby peak from glassy carbon). The limited number of peaks in the diffractograms depends especially on the nature of the samples (thin film, disordered) [18].

Fig. 7 compares the XRD diffractogram measured for the sample Co(44%)Se(56%) with that for bulk CoSe (purity >99%, Alfa Aesar), and a clear mismatch is apparent for the peak near 33.5°. The measured peak position for bulk CoSe matches with the CoSe reference pattern from the Powder Diffraction File (PDF) database [17]; also the XRD peaks due to quartz in the composite sample (Co(44%)Se(56%) plus quartz) match with those from the internal standard for quartz. These observations help remove any speculation that the peak shift could be due to problems with sample alignment; accordingly we believe the peak shift from bulk CoSe is associated with the

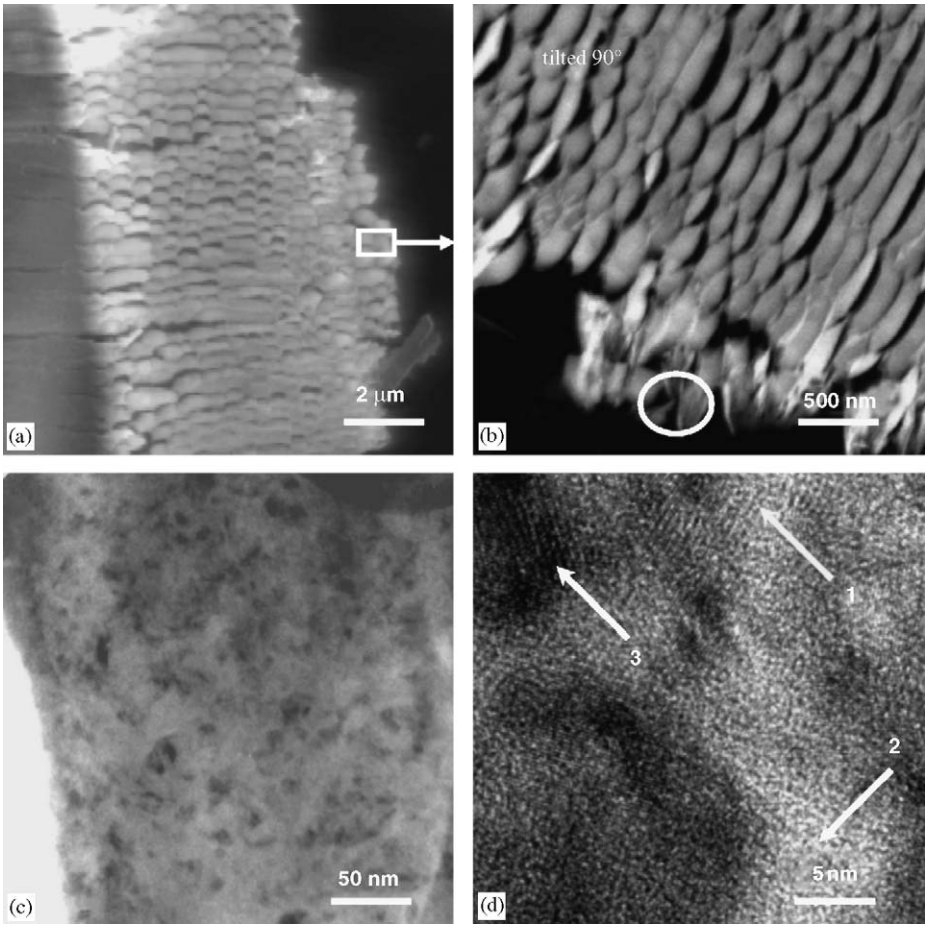

Fig. 3. Sectioned sample of composition Co(44%)Se(56%) at progressively higher magnifications: (a) SEM image from area marked in Fig. 1. The other images are from TEM. The rectangular area marked in (a) indicates the region magnified in (b); the area marked in (b) is magnified in (c) and (d).

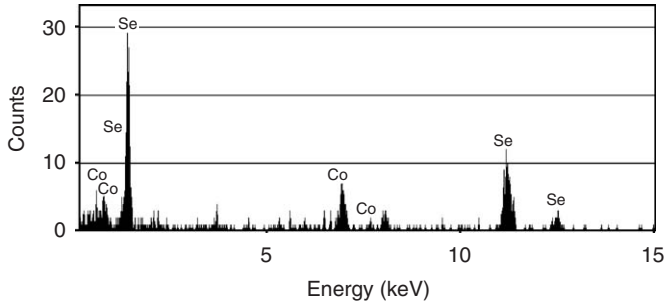

Fig. 4. EDX spectrum from a "black-dot" region.

non-stoichiometric nature of the nanoparticles in the thin film. The peak shift to higher 2θ for the film is consistent with the tendency for d-spacings to decrease with decrease in Co content, as is apparent from Table 1.

The consistency between the conclusions from TEM and XRD for the thin-film sample Co(44%)Se(56%) is made in two ways. First, Fig. 8 compares the measured XRD pattern from this sample with simulations using Powdercell (Powder Cell for Windows, Version 2.4, Federal Institute for Materials Research and Testing, Germany) after inputting the structural parameters for Co_7Se_8 determined by Garcia et al. [15]. The broadening of the peaks from the thin films is expected given the nanocrystalline nature of the originating components, and hence this provides consistency with the conclusion reached by TEM. A second comparison between TEM and XRD is given in Fig. 9, where the d-spacings measured by TEM for individual nanocrystallites in the thin film are plotted as vertical lines on the XRD pattern. The data are compared with the measured diffractogram for the Co(44%)Se(56%) sample, and the distribution of lines (from the separately measured d-spacings) relates well to the experimental peaks, while a considerable discrepancy is seen with the diffractogram measured for (hexagonal) CoSe.

3.3. Thin-film structure

The structural aspects for the thin films discussed in this paper range from the more mesoscopic columnar structure, dependent on the deposition process, to the structure inside the columns which involves nanocrystalline Co–Se particles embedded within a Se-rich matrix. In assessing the nanocrystalline forms, it is useful to compare with the Co–Se bulk crystal structures [16,17]. CoSe, known as freboldite (hexagonal NiAs structure), can be seen as the parent structure for a range of non-stoichio-

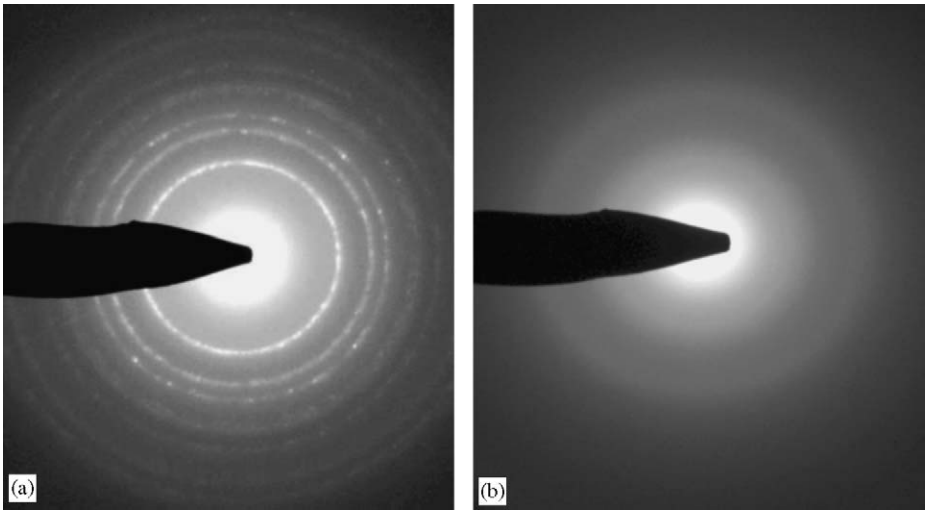

Fig. 5. TEM diffraction patterns from different areas in Fig. 3(c): (a) "black-dot" region showing polycrystalline nature, and (b) "white area" showing amorphous structure.

Table 1
Range of TEM *d*-spacings (in nm) measured for nanocrystallites in thin-film sample of composition Co(44%)Se(56%) and compared against those measured for bulk Co_7Se_8 and CoSe

TEM measured	Co_7Se_8[a]	CoSe[b]
0.2636–0.2659	0.2657	0.2694
0.1986–0.2003	0.1990	0.2022
0.1778–0.1788	0.1785	0.1807
0.1508–0.1514	0.1512	0.1564
0.1486–0.1497	0.1481	0.1500
0.1337–0.1345	—	0.1347
0.1310–0.1319	—	0.1325

[a]Refs. [15,16].
[b]Ref. [17].

metric compounds with cation vacancies. Using the formula $Co_{1-x}Se$, the originating structure is basically maintained for $0<x<0.03$, but the increasing Co vacancies are arranged incommensurately for $0.03<x<0.125$. At $x=0.125$ the formula corresponds to Co_7Se_8, and the structure becomes commensurate and monoclinic. This form continues with more vacancies through to $x=0.25$, which defines the Co_3Se_4 structure. The measured *d*-spacings for Co_7Se_8 and Co_3Se_4 are almost identical [15,16], and as a consequence their diffractograms cannot be distinguished. The similarity in positions for the peak near 33.5°, measured from the different thin-film samples (values range from 33.3° to 33.6°), help make a *prima facie* case that all the Co–Se thin films investigated have similar structures for the nanocrystalline regions (uncertainties in measurements do not allow the identification of any systematic shifts in this peak position which could be related to changing structure for the nanoparticles). The Co–Se phase diagram shows a range of solid solutions with compositions ranging from 50.7 to 59.0 at% Se [19], and the particular ordered structures consistent with the measurements reported here occur within this range.

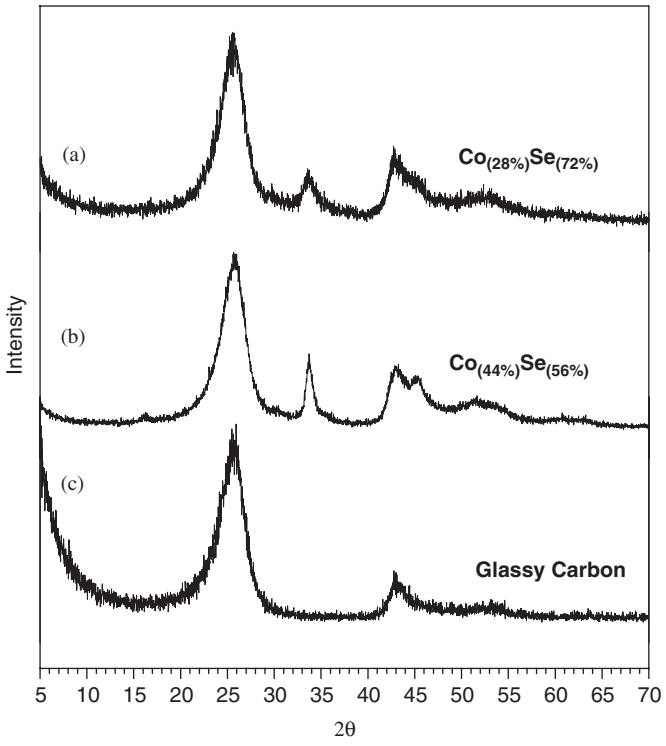

Fig. 6. X-ray diffractograms measured from: (a) thin-film sample of composition Co(28%)Se(72%), (b) thin-film sample of composition Co(44%)Se(56%), and (c) glassy-carbon substrate.

The evidence that the outer regions of the original thin-film surfaces are Se-rich is fully consistent with the Auger measurements reported previously [10]. This opens an interesting mechanistic question since Se itself does not have significant activity for ORR. It is assumed as a working hypothesis that the core of the catalytic activity is associated with nanoparticles whose structures relate to those of monoclinic $Co_{1-x}Se$ ($x=0.125$–0.25), and that the surrounding Se-rich regions have sufficient conductivity to

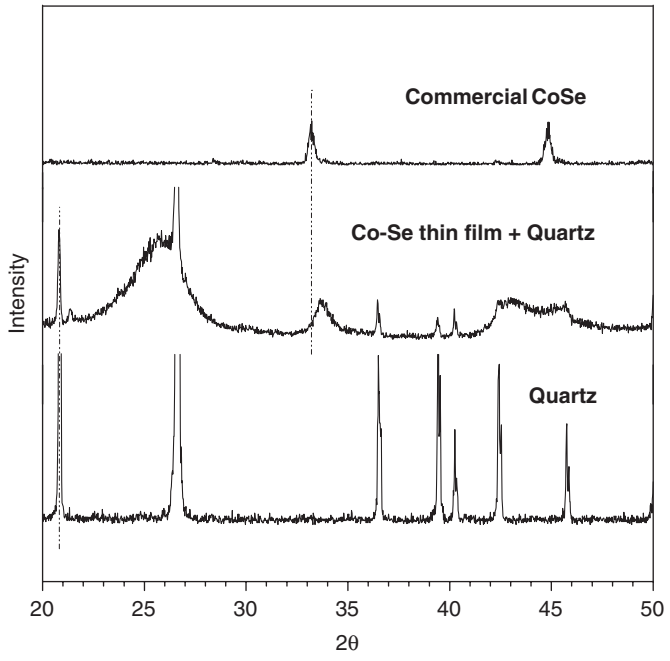

Fig. 7. X-ray diffractograms measured from: (a) commercial CoSe; (b) thin-film sample composition Co(44%)Se(56%) with quartz; and (c) standard quartz sample.

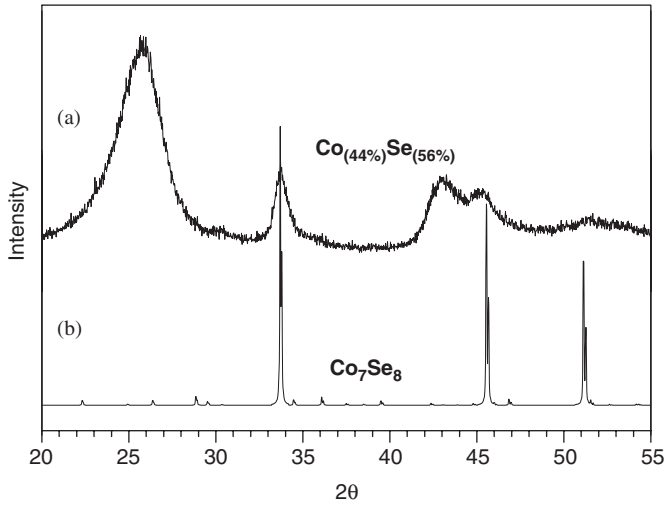

Fig. 8. X-ray diffractograms: (a) measured from thin-film sample of composition Co(44%)Se(56%); and (b) simulated for Co_7Se_8.

effect the electron transfer. That conductivity may originate either intrinsically from local nanoregions of gray Se, or the Se could be doped by small amounts of Co remaining after leaching during the electrochemical characterization. The Se appears to have a dual role of allowing electron transfer during ORR and protecting against corrosion. In relation to the latter point, no O is detected by SAM from the surface region of the thin-film sample after electrochemical testing, although powder samples of commercial CoSe have less protecting Se and show evidence for oxidation.

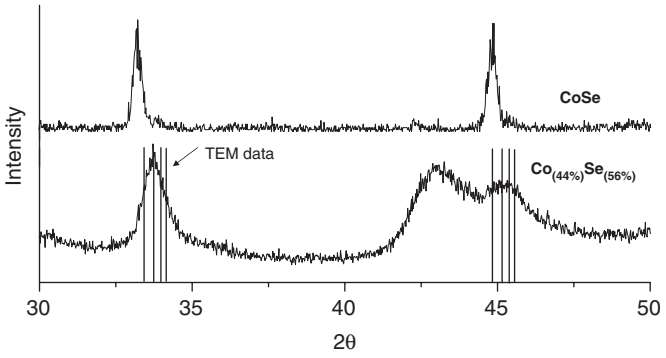

Fig. 9. X-ray diffractograms measured for commercial CoSe and thin-film sample of composition Co(44%)Se(56%), and compared against simulated "peaks" (vertical lines) calculated with the individually measured nanoparticle *d*-spacings (ranges given in Table 1).

4. Concluding remarks

The following summarize some key points from this work:

- High-resolution TEM analyses, combined with SEM and SAM, show that the basic structures of the Co–Se thin films after electrochemical examination for ORR can be interpreted as involving Co–Se nanocrystals embedded into a Se-rich (mainly amorphous) matrix.
- XRD suggests that the Co–Se thin films, over a wide range of overall composition, have the same basic structure, and that the different compositions are set by varying relative amounts for the Co–Se nanocrystals and the Se-rich matrix.
- The TEM and XRD analyses are consistent with the nanosized Co–Se crystallites being described as involving a monoclinic structure related to that of monoclinic $Co_{1-x}Se$ ($x = 0.125$–0.25).
- The Co–Se nanocrystallites involved in ORR are structured differently from those based on chevrel phases.
- For the Co–Se catalysts, questions remain on how the $Co_{1-x}Se$ nanocrystallites are associated with the active site for electron transfer and how the surrounding Se-rich contributes to the whole ORR process.

Acknowledgments

The authors acknowledge the help of Dr. L. Yang (Simon Fraser University) for the HRSTEM experiments, Dr. A. Wong (Faculty of Dentistry, UBC) for use of the ultramicrotome and Ms. M. Mager (Materials Eng., UBC) for EDX measurements. The XRD measurements were made in the Structural Chemistry Facility (Chemistry, UBC), and the SAM measurements were made in the Interfacial Analysis and Reactivity Laboratory (AMPEL, UBC). We thank Drs. B. Patrick, D.V. Shtansky, and D.S.

Wang for helpful discussions. This research was supported by Ballard Power Systems Inc., the United States Department of Energy (contract DE-FC36-03G013107) and the Natural Sciences and Engineering Research Council of Canada.

References

[1] B.M. Barnett, W.P. Teagan, J. Power Sources 37 (1992) 15.
[2] S.G. Chalk, J.F. Millller, F.W. Wager, J. Power Sources 86 (2000) 40.
[3] D. Hart, J. Power Sources 86 (2000) 23.
[4] T.R. Ralph, Platinum Metals Rev. 43 (1999) 14.
[5] D.S. Cameron, Platinum Metals Rev. 49 (2005) 16.
[6] R. Adzic, in: J. Lipkowski, P.N. Ross (Eds.), Recent Advances in Electrocatalysis, Wiley-VCH, New York, 1998, pp. 197–210.
[7] N. Alonso-Vante, H. Tributsch, Nature 323 (1986) 431.
[8] N. Alonso-Vante, M. Fieber-Erdmann, H. Rossner, E. Holub-Krappe, Ch. Giorgetti, A. Tadjeddine, E. Dartyge, A. Fontaine, R. Frahm, J. Phys. IV France 7 (C2) (1997) 887.
[9] N. Alonso-Vante, in: W. Vielstich, A. Lamm, H.A. Gasteiger (Eds.), Handbook of Fuel Cells: Fundamentals, Technology and Applications, Wiley, Chichester, 2003, p. 534.
[10] D. Susac, A. Sode, L. Zhu, P.C. Wong, M. Teo, D. Bizzotto, K.A.R. Mitchell, R.R. Parsons, S.A. Campbell, J. Phys. Chem. B 110 (2006) 10762.
[11] M. Ohring, Materials Science of Thin Films Deposition and Structure, Academic Press, San Diego, 2002.
[12] S.M. Rabchynski, D.K. Ivanou, E.A. Streltsov, Electrochem. Commun. 6 (2004) 1051.
[13] T. Ishiyama, T. Tanaka, Anal. Chem. 68 (1996) 3789.
[14] E.A. Streltsov, S.K. Poznyak, N.P. Osipovich, J. Electroanal. Chem. 518 (2002) 103.
[15] F.J. García-García, A.K. Larsson, L. Norèn, R.L. Withers, Solid State Sci. 6 (2004) 725.
[16] L. Norèn, R.L. Withers, F.J. García-García, A.K. Larsson, Solid State Sci. 4 (2002) 27.
[17] ICDD (International Center for Diffraction Data) PDF 00-089-2004.
[18] B.D. Cullity, Elements of X-ray Diffraction, Addison-Wesley Pub. Co., London, 1978.
[19] T.B. Massalski, Binary Alloy Phase Diagrams, ASM International, Materials Park, OH, 1990, pp. 1235-1237.